Relativistic Quasimonoenergetic Positron Jets from Intense Laser-Solid Interactions

Hui Chen,[1] S. C. Wilks,[1] D. D. Meyerhofer,[2,3] J. Bonlie,[1] C. D. Chen,[1] S. N. Chen,[1] C. Courtois,[4] L. Elberson,[1] G. Gregori,[5] W. Kruer,[1] O. Landoas,[4] J. Mithen,[5] J. Myatt,[2] C. D. Murphy,[5] P. Nilson,[2] D. Price,[1] M. Schneider,[1] R. Shepherd,[1] C. Stoeckl,[2] M. Tabak,[1] R. Tommasini,[1] and P. Beiersdorfer[1]

[1]*Lawrence Livermore National Laboratory, Livermore, California 94551, USA*
[2]*Laboratory for Laser Energetics, University of Rochester, Rochester, New York 14623, USA*
[3]*Department of Mechanical Engineering and Physics, University of Rochester, Rochester, New York 14623, USA*
[4]*CEA, DAM, DIF, F-91297 Arpajon, France*
[5]*Clarendon Laboratory, University of Oxford, OX1 3PU, United Kingdom*

(Received 15 January 2010; published 1 July 2010)

Detailed angle and energy resolved measurements of positrons ejected from the back of a gold target that was irradiated with an intense picosecond duration laser pulse reveal that the positrons are ejected in a collimated relativistic jet. The laser-positron energy conversion efficiency is $\sim 2 \times 10^{-4}$. The jets have $\sim$20 degree angular divergence and the energy distributions are quasimonoenergetic with energy of 4 to 20 MeV and a beam temperature of $\sim$1 MeV. The sheath electric field on the surface of the target is shown to determine the positron energy. The positron angular and energy distribution is controlled by varying the sheath field, through the laser conditions and target geometry.

DOI: 10.1103/PhysRevLett.105.015003 PACS numbers: 52.38.Ph, 52.59.−f

Relativistic positrons and positron jets are believed to exist in many astrophysical objects and are invoked to explain energetic phenomena related to gamma ray bursts and black holes [1–4]. On Earth, positrons from radioactive isotopes or accelerators are used extensively at low energies (sub-MeV) in areas related to surface science [5–8], positron emission tomography [9], basic antimatter science such as antihydrogen experiments [10,11], Bose-Einstein condensed positronium [12], and basic plasma physics [13]. Experimental platforms capable of producing the high-temperature positrons and high-flux positron jets [14] required to simulate astrophysical positron conditions have so far been absent. MeV temperature jets of positrons and electrons produced in these experiments provide a first step towards evaluating the physics models used to explain some of the most energetic phenomena in the Universe.

The pair producing mechanisms in intense laser-plasma interactions have been studied theoretically [15] and demonstrated experimentally in previous ''proof-of-principle'' experiments [16–18]. When intense lasers interact with solid targets a large number of fast electrons (>MeV) are created. These electrons create MeV bremsstrahlung photons in the target that, in turn, produce electron-positron pairs through the Bethe-Heitler process [15,19,20], unlike the direct laser pair production in vacuum which occurs via multiphoton absorption [21]. To date the angular distribution of the positrons ejected from the rear of the target and the source of the quasimonoenergetic nature of the observed positron energy distribution has been unknown. Here we present the first observations that the positrons are ejected in a well-defined cone from the back of the target, accelerated by several MeV due to the sheath field on the rear of the target. We demonstrate this by varying the transverse size of the target and the energy of the laser, both of which change the sheath field and influence the jet energies.

The electron-positron pair creation experiments reported here were performed using 1–10 picosecond laser pulses of 1.054 μm wavelength from the Titan laser [22] at the Lawrence Livermore National Laboratory and the OMEGA EP laser [23] at the University of Rochester's Laboratory for Laser Energetics. Laser energies from 100 to 850 J were focused into 8 (on Titan) to 50 (on OMEGA EP) micrometer diameter spots producing peak laser intensities from 1×10^{19} to 5×10^{20} W/cm^2. All targets were 1 mm thick solid gold with diameters between 1 and 20 mm. The experimental configuration is shown in Fig. 1. The positrons, electrons, and protons produced during the laser-target interaction were measured simultaneously using three absolutely calibrated electron-positron-proton spectrometers (EPPS) [24]. They were placed $\sim$20 cm from the target at various angles to measure the energy spectrum of the electrons and positrons.

In the experiments, quasimonoenergetic, beamlike positron jets were observed. The positron energy spectra are shown in Fig. 2 for six shots with different laser and target conditions that controlled the positron peak energy. The energy of the peak (E_{peak}) of the positron distribution varied from 3 to 19 MeV, with an energy spread from 57% to 15%, equivalent to $E_{\text{peak}}/E_{\text{FWHM}} = 1.8$ to 6.9. The shot conditions are summarized in Table I.

The peak energy shift and the beamlike nature of the positron spectra arise due to sheath field effects from the rear of the target. The sheath field is established by the initial escaping electrons and the resulting electron cloud that forms around the target. It has been confirmed by proton or ion acceleration [25–27]. Since there are several orders of magnitude more electrons than positrons, the

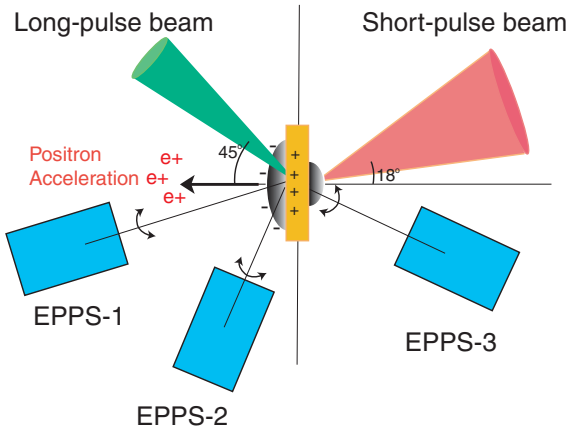

FIG. 1 (color). Experimental setup. The short pulse irradiates the target at 18° relative to target normal. The long-pulse (3 ns square pulse) laser irradiates the rear of the target at 45° for some shots. The long pulse was shot 2 ns before the short-pulse laser. The long-pulse focal spot was about 600 μm diameter centered on the short-pulse focal spot. The laser produced electrons establish a sheath field at the rear of the target that accelerates the positrons. This field can be controlled by the long-pulse laser injection as well as the target surface area variation.

positrons play no role in the sheath formation. As the hot electrons that are responsible for the potential leave the target, it takes less than a few tens of fs to build up a MV/μm field on the rear target surface. The majority of the positrons pass through this sheath field as they leave the target, gaining an energy equal to the potential of the sheath. This results in a shift of positron energy distribution to higher energies. This process is confirmed by two-dimensional hybrid particle simulations which show that the sheath is quickly set up for the positrons to go through,

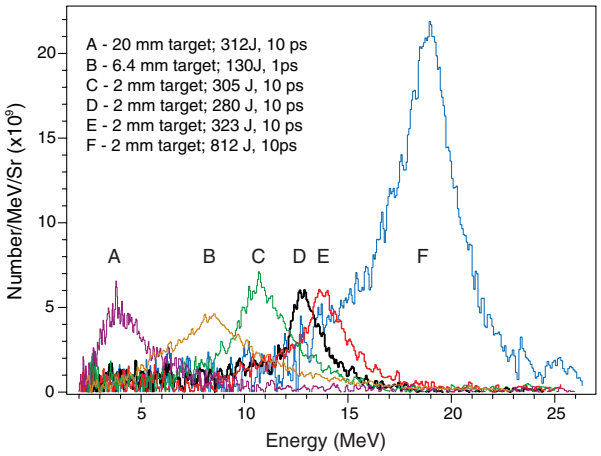

FIG. 2 (color). Positron energy distributions for six laser shots labeled from A to F. The target and laser conditions are listed. Shots A–E were from the Titan laser and shot F from the OMEGA EP laser. All spectra were obtained with the EPPS normal to the back of the target. Shot C had a 7 J, 3 ns long-pulse shot at the rear of the target prior the short pulse laser.

even if the electrons and positrons are launched at the same time. To verify this effect experimentally, we decreased the sheath strength at the back of the target by increasing the scale length of the plasma at the rear of the target [25,26]. This was accomplished by irradiating the rear side of the target with a second, long (ns) laser pulse (in shot C), a technique that has been demonstrated in [28]. This resulted in a ~3 MeV decrease in the peak energy of positron distribution. (Shot C vs shot E in Table I.)

The target size affects the positron acceleration field. Larger targets reduce the acceleration field so that the observed positron distribution approaches that inside the target. This "low-energy" distribution is determined by the Bethe-Heitler process [18], as shown in Fig. 3. The positron "birth" distribution was simulated using the Monte Carlo code EGSNRC [29] that calculates the Bethe-Heitler pair production and self-consistently treats the attenuation of electrons, photons, and positrons as they propagate through a cold solid target. It does not include the sheath potential effect that causes the additional acceleration of positrons at the rear target surface. The experimental data using a 20 mm diameter target have the lowest peak energy (~4 MeV) and are the closest to the simulated positron distribution peaked at about 2.5 MeV.

The positron beam (jet) energy scales approximately inversely with the surface area of the target for constant laser conditions and target thickness, as shown in the inset of Fig. 3. As the target diameter increases from 1 to 20 mm, the peak positron energy decreases from 18 to 4 MeV. The measured maximum proton energy also decreases from greater than 15 MeV to less than 0.5 MeV as the target diameter increases, consistent with the positron data. Since the electron source is the same for each target, the charge density is reduced as the target area increases, reducing the accelerating field as shown by the shift in the peak of positron energy to lower energies and the decrease in the maximum observed proton energy. This is consistent with the understanding of how the sheath field is generated, as described above.

The jet nature of these quasimonoenergetic positrons is established by measuring the beam angular divergence of electrons and positrons emitted from the rear surface of the target. The divergence half-angles ranged from 17° to 25°, with the smaller angles corresponding to the higher beam energies. Figure 4 shows measurements (for shot B in Fig. 2) of the normalized total positron number as a function of angle with the laser propagation direction at 0° and the target normal direction being −18°. A Gaussian function fit to the data shows a half-width of ~20 ± 5° centered at −10 ± 5°. Fast electrons measured with the EPPS and radiochromic film show (in the inset of Fig. 4) a jetlike distribution similar to the positrons, with half-width of ~25 ± 5° centered at −12 ± 5°.

The physics that determines the electron directionality is different from that of the positrons. Fast electrons accel-

TABLE I. Summary of shot conditions and the ejected positrons for shots A–F. The short-pulse duration for all shots was 10 ps except shot B, which was 1 ps. Columns 2 and 3 are laser parameters: column 2 is the laser energies on target; column 3 the target diameter. Columns 4–8 are the quasimonoenergetic positron jet parameters: column 4 is the total number of positrons in the jet; column 5 is the energy of the peak of the distribution; column 6 is the energy for the full width at half maximum of the distribution; column 7 is the energy spread in percentage; column 8 is the half-angle of the divergence. Columns 9–11 are the derived positron properties: column 9 is the energy conversion efficiency from laser to ejected positrons. Columns 10 and 11 are the derived positron jet temperatures: column 10 is the temperature in the jet longitudinal direction; column 11 is the temperature in the transverse direction. Numbers in parentheses are the best estimated errors to the attached number.

	Laser parameters		Positron jet parameters						Derived quantities	
Shots	E_{Laser} (J)	Φ (mm)	$N_{\text{total } e^+}$	E_{peak} (MeV)	E_{FWHM} (MeV)	Spread (%)	θ^{b} (Degree)	η_{energy} (%)	$T_{\parallel}$ (MeV)	$T_{\perp}$ (MeV)
A	312	20	1.8e10	4.0 (0.1)	2.3 (0.3)	57 (6)	25	0.01	2.9 (0.2)	0.4
B	130	6.4	2.0e10	8.5 (0.2)	3.3 (0.3)	39 (6)	20 (5)	0.03	6.5 (0.6)	1.6
C[a]	305	2	3.0e10	10.8 (0.1)	3.1 (0.1)	29 (2)	18	0.02	4.2 (0.2)	0.8
D	280	2	2.3e10	12.8 (0.1)	1.9 (0.2)	15 (4)	17	0.02	2.5 (0.3)	1.0
E	323	2	2.6e10	13.7 (0.1)	2.8 (0.2)	21 (3)	20	0.04	4.1 (0.2)	1.2
F	812	2	1.8e11	18.7 (0.1)	3.6 (0.2)	19 (2)	17	0.04	4.2 (0.2)	2.0

[a]A 7 J, 3 ns long-pulse injection was shot at the rear of the target before the short pulse to increase the plasma scale length.
[b]Derived from measurements shown in Fig. 4 for shot B. It is derived from two-point measurements from the rest of the shots.

erated in front of the target are directed primarily along the laser axis, driven by the $\mathbf{J} \times \mathbf{B}$ forces along the laser propagation direction as well as by the resonant and Brunel absorption mechanisms that drive electrons along the target normal direction. Positrons are born deep inside the target predominantly from the most energetic electrons. These positrons carry some of the forward momentum of the ''parent'' fast electrons forming an anisotropic distribution [18]. Once outside the target, these positrons are accelerated by the sheath electric field reshaping the positron distribution. This is verified by experiments with 18° and 55° laser incidence relative to target normal direction. It was found that nearer to normal incidence the laser produced less divergent positron beams because there the acceleration direction is better aligned with the original positron momentum gained at birth pointing in the laser propagation direction.

The total number (N) of positrons in the jet is estimated to be on the order of 10^{10} to 10^{11} by integration over the angular spread of the jet. N scales approximately linearly with laser energy as $N \sim (1.5 \times 10^{11}) \times E_{\text{laser}}(\text{kJ})$. The total energy conversion efficiency from laser energy to positrons in the jet is $\sim 2 \times 10^{-4}$. The positron jet current ($\sim$100 A) is far below the Alfvén beam current limit

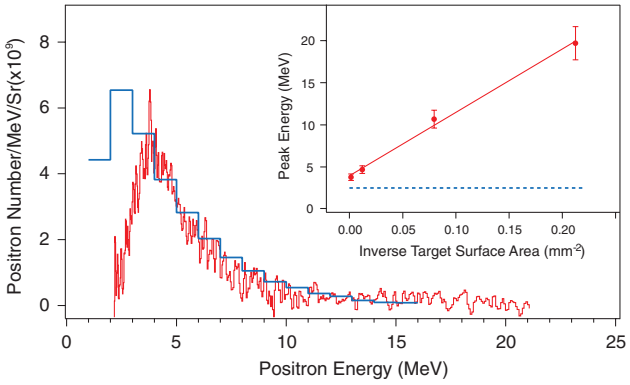

FIG. 3 (color). Positron spectra from 1 mm thick Au target with diameter of 20 mm (red) and from EGS code (blue). The simulation is linearly scaled with an arbitrary factor in the y axis to show its peak energy. The inset shows the peak energy of positrons as a function of the inverse of target surface area. The relation is fitted with a linear function $E \propto 1/S$. The dashed line (blue) represents the peak energy without the acceleration field, calculated from the EGS simulation.

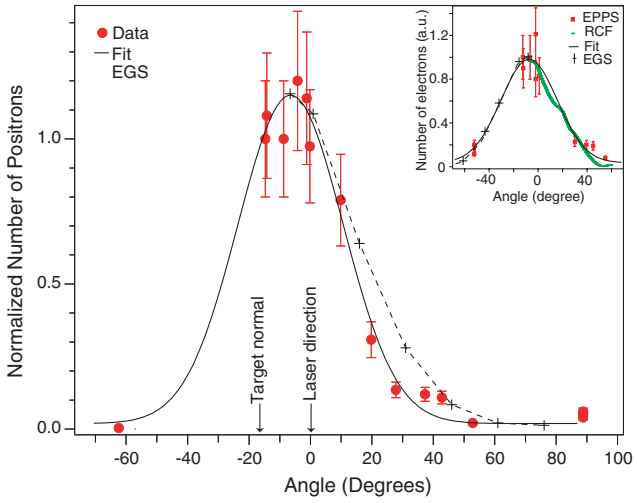

FIG. 4 (color). Normalized total positron number ejected from the back of targets at various angles for 1 mm thick, 6.4 mm diameter targets shot by 1 ps, 130 J laser (shot B in Fig. 2). The data (red dots with error bars) are fit (black) with a Gaussian function. The two arrows mark the laser propagation direction and the target normal direction. The result for the electrons is shown in the inset which includes both EPPS data (red squares) and data from radiochromic film (green dots). It was not possible to measure positrons for angles between $-60°$ and $-20°$ due to the laser beam layout.

(~10 000 A) [30]. The jet is charge-neutralized by the copropagating electrons. The electrons and positrons travel at nearly the velocity of light in the direction of the jet, ahead of the protons and ions that are accelerated by the sheath electric field, forming a non-neutral electron-positron plasma. For the duration of 10 picoseconds (laser duration), these relativistic electrons and positrons occupy a volume of $\sim 3 \times 10^{-3}$ cm^3, from which a positron density of $\sim 10^{13}$/cm^3 and electron density of $\sim 10^{15}$/cm^3 are inferred. EGS simulations show a positron density of $\sim 10^{16}$ cm^{-3} inside of the target.

The positron temperature is determined from the width of the energy spectrum in the jet, longitudinal, direction and from the angular divergence of the jets in the transverse direction. In the longitudinal direction, the temperatures ($T_{\|}$) are between 2 and 6 MeV. In the transverse direction, the temperatures ($T_{\perp}$) are between 0.4 and 2 MeV. The temperatures obtained in the EGS simulations (for shot A, Fig. 3) are 3.4 and 1.4 MeV in the longitudinal and transverse directions, respectively, supporting the experimental data. The copropagating hot electron temperatures are about 3 to 9 MeV with a quasi-Maxwellian distribution [18].

In summary, this is the first description of the fundamental properties of laser-generated positron jets, including the angular distribution, the conversion efficiency, the number, the peak energies, and the temperatures. This Letter clearly demonstrates that the sheath field determines the positron beam energy. The power in these electron-positron jets is about 10^{19} erg/s, i.e., far less than that of astrophysical sources [1–4]. However, the energy flux is of the order of 10^{21} erg/s/cm^2 and sufficient to permit future scaled experiments [31] of astrophysical phenomena. In addition, if the jets can be trapped, for example, in a ''mirror-type'' magnetic field, a stationary high-temperature electron-positron plasma may be created [15]. With the positron beam intensity of about 10^{12} W/cm^2, these positrons may find new applications such as diagnosing high energy density plasmas and providing a source of pulsed, monoenergetic gamma rays for radiography of dynamic processes in materials, as well as provide a platform for the studying the physics of some of the most energetic phenomena in the Universe.

This work was performed under the auspices of the U.S. DOE by LLNL under Contracts No. DE-AC52-07NA27344 and No. DE-FC52-08NA28302 at LLE, and was funded with LLNL LDRD-08-LW-058 and ILSA. G. G., C. M., and J. M. were supported by the EPSRC (#EP/G007187/1) and John Fell Fund. We thank the staff at the LLNL Jupiter Laser Facility and the LLE OMEGA EP laser. We acknowledge support from Roger Van Maren, Don Correll, and Bill Goldstein, and discussions with Peter Norreys and Robert Heeter.

[1] J. Wardle *et al.*, Nature (London) **395**, 457 (1998).
[2] I. F. Mirabel and L. F. Rodriguez, Annu. Rev. Astron. Astrophys. **37**, 409 (1999).
[3] G. Weidenspointner *et al.*, Nature (London) **451**, 159 (2008).
[4] P. Meszaros, Annu. Rev. Astron. Astrophys. **40**, 137 (2002).
[5] A. P. Mills, Science **218**, 335 (1982).
[6] P. J. Schultz and K. G. Lynn, Rev. Mod. Phys. **60**, 701 (1988).
[7] A. W. Hunt *et al.*, Nature (London) **402**, 157 (1999).
[8] D. W. Gidley, H.-G. Peng, and R. S. Vallery, Annu. Rev. Mater. Res. **36**, 49 (2006).
[9] M. E. Raichle, Nature (London) **317**, 574 (1985).
[10] M. Amoretti *et al.*, Nature (London) **419**, 456 (2002).
[11] G. Gabrielse *et al.*, Phys. Rev. Lett. **89**, 213401 (2002).
[12] P. M. Platzman and A. P. Mills, Phys. Rev. B **49**, 454 (1994).
[13] C. M. Surko and R. G. Greaves, Phys. Plasmas **11**, 2333 (2004).
[14] M. H. Thoma, Rev. Mod. Phys. **81**, 959 (2009), and references cited within.
[15] J. W. Shearer *et al.*, Phys. Rev. A **8**, 1582 (1973); P. L. Shkolnikov *et al.*, Appl. Phys. Lett. **71**, 3471 (1997); D. A. Gryaznykh, Y. Z. Kandiev, and V. A. Lykov, JETP Lett. **67**, 257 (1998); E. P. Liang, S. C. Wilks, and M. Tabak, Phys. Rev. Lett. **81**, 4887 (1998); B. Shen and J. Meyer-ter-Vehn, Phys. Rev. E **65**, 016405 (2001); K. Nakashima and H. Takabe, Phys. Plasmas **9**, 1505 (2002); V. I. Berezhiani, D. P. Garuchava, and P. K. Shukla, Phys. Lett. A **360**, 624 (2007); J. Myatt *et al.*, Phys. Rev. E **79**, 066409 (2009).
[16] T. Cowan *et al.*, Laser Part. Beams **17**, 773 (1999).
[17] C. Gahn *et al.*, Appl. Phys. Lett. **77**, 2662 (2000).
[18] Hui Chen *et al.*, Phys. Rev. Lett. **102**, 105001 (2009).
[19] W. Heitler, *The Quantum Theory of Radiation* (Clarendon Press, Oxford, 1954).
[20] K. Nakashima and H. Takabe, Phys. Plasmas **9**, 1505 (2002).
[21] D. L. Burke *et al.*, Phys. Rev. Lett. **79**, 1626 (1997).
[22] B. C. Stuart *et al.*, in *Conference on Lasers and Electro-Optics/Quantum Electronics and Laser Science Conference and Photonic Applications Systems Technologies, Technical Digest (CD)* (Optical Society of America, Long Beach, CA, 2006), paper JTuG3.
[23] L. J. Waxer *et al.*, Opt. Photonics News **16**, 30 (2005).
[24] H. Chen *et al.*, Rev. Sci. Instrum. **79**, 10E533 (2008).
[25] S. P. Hatchett *et al.*, Phys. Plasmas **7**, 2076 (2000).
[26] S. C. Wilks *et al.*, Phys. Plasmas **8**, 542 (2001).
[27] R. A. Snavely *et al.*, Phys. Rev. Lett. **85**, 2945 (2000).
[28] A. J. Mackinnon *et al.*, Phys. Rev. Lett. **86**, 1769 (2001).
[29] I. Kawrakow and D. W. O. Rogers, National Research Council of Canada Report No. PIRS-701, 2006.
[30] H. Alfvén, Phys. Rev. **55**, 425 (1939).
[31] B. A. Remington, D. Arnett, R. P. Drake, and H. Takabe, Science **284**, 1488 (1999).